JOURNAL OF GEOPHYSICAL RESEARCH, VOL. 103, NO. C3, PAGES 5563–5575, MARCH 15, 1998

Observations of the polarization of light reflected from sea ice

Donald K. Perovich

U.S. Army Cold Regions Research and Engineering Laboratory, Hanover, New Hampshire

Abstract. As part of a large, interdisciplinary program investigating the electromagnetic properties of sea ice, we made spectral measurements of the albedo, reflectance, and Stokes vector of the reflected radiance field. The overall program encompassed observations of sea ice physical properties, optical properties and microwave properties, plus an extensive modeling effort. Measurements were made of an evolution sequence including young sea ice, pancake ice, snow-covered ice, first-year ice, and ponded ice. The effects of surface roughness were investigated by artificially roughening part of a 31-cm-thick, smooth, young ice sheet. Spectral and total albedos were sensitive to surface conditions, consistent with earlier studies. Stokes vector observations exhibited the greatest variability in the plane of incidence of the solar beam. Reflectances at 0° azimuth increased sharply with zenith angle. Smoother surfaces, such as melt ponds, pancakes and bare ice, exhibited a larger increase than the snow-covered cases with their "rougher" surfaces. Since the solar zenith angle was close to Brewster's angle, specularly reflected light was highly polarized. In the "smooth" ice cases, there was significant polarization associated with the increase in reflectance, implying a substantial contribution from specular reflection. This contribution was greater at longer wavelengths, where specular reflection was a larger component of the reflected radiance. Away from the plane of incidence, the Stokes vector showed little angular variation, and the reflected light at these angles was largely unpolarized.

1. Introduction

An understanding of the reflection of visible and near-infrared light from a sea ice cover is important for climatological studies involving the energy balance of the polar regions, for the interpretation of remote sensing imagery, and for analyzing radiative transfer processes in sea ice. Since solar radiation drives the summer melt cycle of sea ice, understanding the distribution of incident solar radiation between reflection, absorption, and transmission is critical in determining the energy balance of the ice cover [*Maykut and Untersteiner*, 1971; *Ebert and Curry*, 1993; *Ebert et al.*, 1995]. The ability to interpret remote sensing data is required to investigate the distribution of solar radiation over larger scales. Sea ice radiative transfer models [*Grenfell*, 1983, 1991; *Perovich*, 1990; *Jin et al.*, 1994] are needed to address issues involving the spatial and temporal variability of sea ice optical properties.

Because of their importance to the heat and mass balance of the ice there is an extensive database of wavelength-integrated and spectral albedos. Changes in albedo during the melt season [*Langleben*, 1969; 1971; *Grenfell and Maykut*, 1977; *Grenfell and Perovich*, 1984; *Buckley and Trodahl*, 1987; *Perovich*, 1994] and fall freeze-up [*Perovich*, 1991] have been studied. These studies have established that sea ice albedos depend strongly on surface conditions and on the amount and distribution of brine pockets and air bubbles in the interior of the ice. Modeling efforts are underway to quantify the relationship between ice optical and physical properties but are hampered by limited information on scattering processes within the ice.

For climate studies it is necessary to extend these surface-based measurements of albedo to larger scales by using remote sensing data. Optical remote sensing instruments typically have a narrow field of view and measure the reflected radiance at a particular angle. Thus information is needed on the bidirectional reflectance distribution function (BRDF), the angular distribution of reflected radiance as a function of solar angle. Such observations have been made for snow [*Dirmhirn and Eaton*, 1975; *Kuhn*, 1985; *Steffen*, 1987; *Dozier et al.*, 1988; *Grenfell et al.*, 1994] and sea ice [*Schlosser*, 1988; *Perovich*, 1991, 1994]. Reflectances from snow are typically isotropic in all but the forward direction, where for large solar zenith angles, reflectances can increase by a factor of 4 [*Grenfell et al.*, 1994]. Observations of sea ice have shown strong anisotropy in the forward direction for bare ice and for ponded ice.

While there are a large number of observational data available on sea ice albedos and a few measurements of reflectance, there is very little information regarding the polarization of the reflected light. *Perovich* [1994] examined linear polarization of light reflected from first-year ice and found that polarization was greatest in the plane of reflection at longer wavelengths for smooth surfaces. *Hunt et al.* [1994] and *Miller et al.* [1996, 1997] made laboratory measurements of the polarization of light scattered by sea ice samples.

The work described in this paper was performed as part of a large, interdisciplinary program investigating the electromagnetic properties of sea ice. A primary goal of this program was understanding the mechanisms linking the morphological and physical properties of sea ice to its electromagnetic properties. In this paper we examine light reflected from sea ice at visible and near-infrared wavelengths from 400 to 1000 nm. The reflected light is examined at four levels of increasing detail: total albedo, spectral albedo, reflectance, and Stokes vector. The Stokes vector of reflected light is presented for selected azimuth and zenith angles. Stokes vector data of the reflected light field could be useful in ice type discrimination. Such data

Paper number 97JC01615.

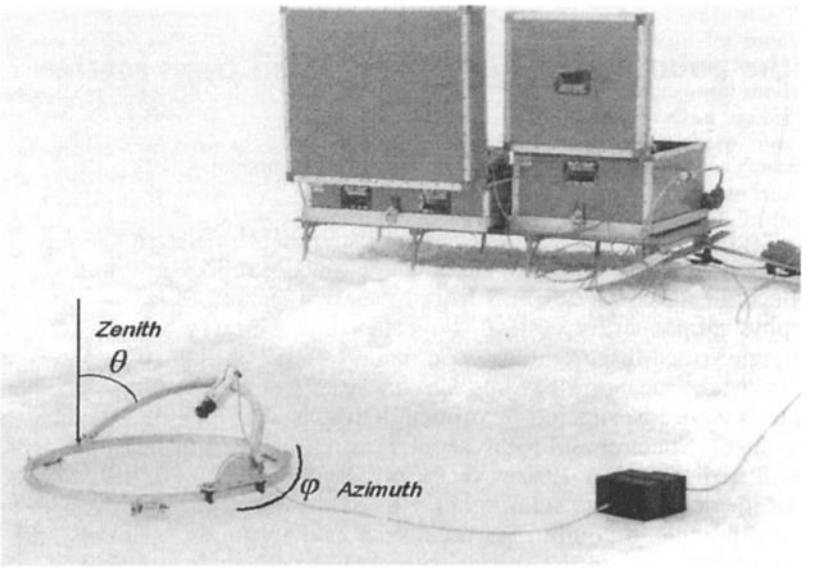

Figure 1. The reflectance ring and "Stokesmeter." The surface was 170-cm-thick cold, bare ice.

may also provide a means of differentiating between backscatter from the surface of the ice and scattering from within the volume of the ice, thus lending insight into radiative transfer in sea ice. This analysis is done for six distinct cases encompassing a representative range of first-year ice types including (1) young congelation ice, (2) pancake ice, (3) cold-snow-covered first-year ice, (4) melting-snow-covered first-year ice, (5) cold, bare first-year ice, and (6) ponded first-year ice. These six cases represent a possible evolutionary sequence for first-year ice from initial growth to summer melt. In addition, observations of young ice with a smooth and a rough surface are compared in order to determine the effects of roughness on the magnitude and polarization of reflected light.

2. Experimental Procedure

The observation program consisted of both laboratory and field measurements. The laboratory work was performed in an outdoor sea ice pond located at the Cold Regions Research and Engineering Laboratory in Hanover, New Hampshire. The sea ice pond is 8 m wide by 20 m long by 2 m deep and has full refrigeration capability. The facility is especially useful for studying young ice under controlled conditions. The measurements of young columnar ice, pancake ice, and smooth and rough young ice were made at this facility during January 1994 and January 1995. The sea ice pond is not suitable for investigating thick ice (>1 m), and field studies were needed to supplement the laboratory results. The field work was conducted in shore-fast ice near Barrow, Alaska, in May 1994 and June 1995.

Two instruments were used to make measurements of the reflected light. Total albedos, integrated over wavelengths from 300 to 3000 nm, were measured using a Kipp radiometer. All spectral measurements were made using a Spectron Engineering SE590 spectroradiometer. This instrument used a diffraction grating to disperse the spectrum into 200 discrete channels between 400 and 1000 nm and used a silicon photodiode array as a detector. Different foreoptics were mounted on the instrument for the albedo and the Stokes vector measurements.

Albedo measurements were made using a hemispherical diffuser on the instrument to measure irradiance. The angular response of the diffuser deviated from a true cosine response by less than 8%. The instrument was placed on a 1.5-m-long arm to avoid shadowing effects and was mounted on a tripod for easy leveling. Spectral albedos $\alpha(\lambda)$ were determined by pointing the detector upward to measure the incident irradiance $F_i(\lambda)$ and downward to measure the reflected irradiance $F_r(\lambda)$ and then taking the ratio $\alpha(\lambda) = F_r(\lambda)/F_i(\lambda)$. Experimental uncertainties in albedo were less than 0.03.

The equipment configuration for the Stokes vector measurements is displayed in Figure 1. For the Stokes measurements the cosine collector was replaced with the "Stokesmeter" shown in Figure 1 suspended from the center of the ring. The Stokesmeter was modeled after a microwave instrument developed by T. C. Grenfell [*Grenfell*, 1994] and consisted of three elements mounted in a light-tight cylinder: the reflected light encountered first a circular polarizer, then a linear polarizer and finally a 1° field of view lens. The light was transmitted to the spectroradiometer via a 2-m-long glass fiber-optic cable. The linear polarizer worked over the full wavelength range of the instrument, while the circular polarizer had a more limited range of 425–700 nm and a center wavelength of 550 nm. The Stokesmeter was mounted on a rotating ring that could easily be adjusted to different azimuth (ϕ) and zenith (θ) angles. The ring configuration had the advantage of viewing approximately the same portion of the surface as the azimuth and zenith angles were changed. It was, however, limited to a maximum zenith angle of 70°.

Stokes vector measurements were typically made at zenith angles of 0°, 30°, 45°, and 60° for several azimuth angles (ϕ = 0°, 45°, 90°, 135°, 180°). Earlier studies of the bidirectional reflectance distribution function for snow and sea ice [*Steffen*, 1987; *Dozier et al.*, 1988; *Schlosser*, 1988; *Perovich*, 1991, 1994] showed that the greatest variation in reflectance was in the plane of incidence (ϕ = 0°), and accordingly the measurement density was increased to every 10° of zenith angle from 0° to 70°. Reference values of reflected radiance R_R from a Spectralon white Lambertian reflectance standard (reflectance =

0.98–0.99) were also recorded and used to normalize the Stokes vector measurements.

The Stokes vector was determined at each angle by measuring six spectral scans. Different polarizations P of the reflected light were measured for each of the scans by adjusting the circular and linear polarizers. The measurement sequence and the orientation of the linear and circular polarizers are summarized in Table 1. These six measurements, along with the reference reading R_R, were combined to determine the four components of the Stokes vector using the following relationships [*Bohren and Huffman*, 1983]:

$$I = (I_h + I_v)/R_R$$

$$Q = (I_h - I_v)/R_R$$

$$U = (I_{45} - I_{-45})/R_R$$

$$V = (I_R - I_L)/R_R$$

The degree of linear polarization is defined as

$$\text{DLP} = (Q^2 + U^2)^{1/2}/I$$

In this formulation, I is the reflectance normalized to a white Lambertian reference standard. Thus the combined set of I measurements at different azimuth and zenith angles is a component of the bidirectional reflectance distribution function BRDF. Normalized in this fashion, I at a particular angle can be greater than 1. However, the integral of I over angle must be less than or equal to 1. The surfaces studied in this experiment were free of azimuthally oriented features, so the BRDF can be simplified and expressed as

$$R(\theta_0, \theta, \phi, \lambda) = I(\theta_0, \theta, \phi, \lambda) = \frac{dI_r(\theta, \phi, \lambda)}{\mu_0 dF_0(\theta_0, \phi, \lambda)}$$

where the units of R are reciprocal steradians, θ_0 is the solar zenith angle, θ and ϕ are the detector zenith and azimuth angles, $\mu_0 = \cos\theta_0$, $I_r(\theta, \phi, \lambda)$ is the reflected spectral irradiance, and $F_0(\theta_0, \phi, \lambda)$ is the spectral incident irradiance [*Warren*, 1982; *Perovich*, 1994]. Reflectance can be directly compared with the hemispherical albedo by combining the BRDF with the spectral albedo to define the anisotropic reflectance function f:

$$f(\theta_0, \theta, \phi, \lambda) = \frac{\pi R(\theta_0, \theta, \phi, \lambda)}{\alpha_0(\theta_0 \lambda)}$$

The optical system was designed for fast operation so that a measurement sequence could be completed before the solar angle or incident irradiance changed appreciably. Total albedos were measured in a few seconds, while spectral albedo measurements were made in about 30 s. Stokes measurements at a single angle took roughly 1 min, and roughly 30 min were needed to complete a full set of many different angles.

An important supplement to the optical measurements was characterizing the surface conditions and the physical properties of the sea ice. Ice surface conditions, including roughness and the presence of snow or water, strongly impact light reflection [*Grenfell and Maykut*, 1977; *Grenfell and Perovich*, 1984; *Perovich*, 1996]. If snow was present, its depth, density, and grain size were measured. For ponded ice the depth of the melt pond was measured, and for bare ice the roughness was qualitatively described. The description of the ice interior included vertical profiles of temperature, salinity, and brine volume obtained from ice core analysis [*Weeks and Ackley*, 1982; *Tucker et al.*, 1987]. Horizontal and vertical thin sections were used to determine ice crystallography and to generate estimates of the size distributions of air and brine inclusions.

Table 1. Measurement Sequence for Stokes Vector

Sequence	Polarizer Setting, deg: Linear	Polarizer Setting, deg: Circular	Polarization	Symbol
1	0	0	vertical	I_v
2	45	45	plus 45°	I_{45}
3	90	90	horizontal	I_h
4	−45	−45	minus 45°	I_{-45}
5	0	45	left circular	I_L
6	0	−45	right circular	I_R

Values are normalized to reference reflectances R_r.

3. Results and Discussion

3.1. Incident Irradiance

The optical measurements were made under sunny skies with solar zenith angles between 55° and 70° (Table 2). Both the total and the diffuse incident spectral irradiance were measured. The diffuse values were determined by obscuring the direct solar beam with a small, 4-cm-diameter opaque disk. The incident spectral irradiance measured at Barrow, Alaska, for a solar zenith angle of 56° is plotted in Figure 2a. While the magnitude varied somewhat for the other cases, the spectral dependence of incident irradiance was quite similar. The incident irradiance increases with wavelength to a maximum value of 1.7 W m^{-2} nm^{-1} at 470 nm, then decreases to a minimum value of 0.5 W m^{-2} nm^{-1} at 940 nm. The absolute uncertainty in the incident irradiance measurements is approximately 15%. The ratio of the diffuse/total incident irradiance is plotted as a function of wavelength in Figure 2b. This ratio decreases with wavelength, following a power law with an exponent E of −2.8 and a correlation coefficient of 0.99. The decrease with wavelength is less than that predicted by Rayleigh scattering ($E = -4$) and less than that observed by *Grenfell et al.* [1994] at South Pole ($E = -3.26$) and Vostok ($E = -3.33$), implying that particles made a significant contribution to atmospheric scattering in our observations.

3.2. Physical Properties

An important element of this work was physically characterizing the snow and ice that was studied optically (Table 2). Plates 1a to 1f show surface conditions for the six ice types studied: young columnar ice, pancake ice, dry snow, melting snow, bare ice, and ponded ice. Significant variability in surface conditions is evident in these photographs from the rough, diffusely scattering snow to the smooth and highly specularly reflecting pancake and melt pond cases. Spectral variations in reflected light are also apparent at visible wavelengths, as is evidenced by the gray pancakes, the blue pond, and the white snow-covered ice.

Scattering within the medium was determined by the physical properties of the interior of the snow and ice. The young ice was 15 cm thick with temperatures in the −5°C to −10°C range and salinities between 4‰ and 6‰. The crystal structure of the ice consisted of a few millimeters of granular ice at the surface with a 3-cm-thick layer of transitional columnar ice

Table 2. Summary of Selected Results With the Detector at 0° Azimuth Angle and Either 50° or 60° Elevation

Type	Young Ice	Pancakes	Dry Snow	Melting Snow	Cold, Bare Ice	Melt Pond	Smooth Ice	Rough Ice
				Conditions				
Location	Hanover	Hanover	Hanover	Barrow	Barrow	Barrow	Hanover	Hanover
Date	Jan. 26, 1994	Jan. 26, 1995	Feb. 7, 1995	June 8, 1995	May 3, 1994	June 9, 1995	Jan. 16, 1994	Jan. 16, 1994
Time, LT	1350	1145	1150	1120	1140	1725	1110	1350
Solar zenith angle, deg	67	63	59	56	61	57	66	69
Specular polarization	0.73	0.84	0.94	0.98	0.9	0.97	0.76	0.66
Sky*	BC	BC	BC	BC	LH	BC	BC	BC
Detector zenith angle, deg	60	60	60	50	60	50	60	60
Snow depth H_s, cm	0	0	18.5	6	0	0	0	0
Ice thickness H_i, cm	15	15	0	162	170	160	31	31
Pond depth H_p, cm	0	0	0	0	0	6	0	0
				Albedo				
Total	0.32	0.18	0.74	0.60	0.40	0.16	0.26	0.40
450 nm	0.42	0.30	0.92	0.82	0.61	0.31	0.42	0.50
550 nm	0.42	0.32	0.93	0.83	0.62	0.35	0.43	0.50
700 nm	0.38	0.29	0.94	0.80	0.49	0.26	0.34	0.43
900 nm	0.26	0.18	0.89	0.65	0.31	0.12	0.20	0.33
				Anisotropic Reflectance Function: $\theta = 0°$, $\phi = 0°$				
450 nm	0.71	0.74	1.09	0.82	0.93	0.49	0.74	0.76
550 nm	0.71	0.71	1.05	0.80	0.94	0.52	0.72	0.75
700 nm	0.67	0.64	1.02	0.78	0.86	0.39	0.65	0.74
900 nm	0.44	0.39	1.01	0.72	0.62	0.16	0.41	0.67
				Anisotropic Reflectance Function: $\theta = 60°$, $\phi = 0°$				
450 nm	2.93	4.26	1.38	1.19	1.79	1.49	4.47	1.76
550 nm	3.14	4.52	1.36	1.20	1.90	2.36	4.62	1.86
700 nm	3.42	5.32	1.31	1.22	2.24	5.88	5.27	2.11
900 nm	4.28	9.10	1.32	1.31	3.12	27.15	7.77	2.59
				Degree of Linear Polarization: $\theta = 50°, 60°$, $\phi = 0°$				
450 nm	0.56	0.69	0.05	0.02	0.26	0.53	0.76	0.04
550 nm	0.56	0.70	0.06	0.02	0.26	0.70	0.74	0.04
700 nm	0.58	0.73	0.06	0.02	0.30	0.90	0.77	0.05
900 nm	0.68	0.80	0.06	0.01	0.39	0.98	0.83	0.06

*Sky conditions are BC, brilliantly clear, and LH, light haze with Sun clearly visible.

underneath and then 12 cm of c axis horizontal columnar ice. The pancake ice was also 15 cm thick, but in this case the top 10 cm of the ice cover was granular and the remaining 5 cm was transitional columnar. The surface of the pancake ice had melted and refrozen, giving it a smooth and glazed appearance. In the dry snow case the snow depth was 19 cm and the density was 0.22 g cm^{-3}. The snow grains were well rounded and were approximately 0.25 mm in diameter. Since the snow was optically thick, the fact that it was on a substrate of frozen ground rather than ice did not impact the reflection measurements. This snow did differ somewhat from the typical Arctic snow cover, since it had a smaller density and was not wind packed. Observations of melting snow on sea ice were made near Barrow, Alaska, in June. The snow depth was 6 cm, and the density was 0.41 g cm^{-3}. The snow grains were rounded and quite large, ranging from 3 to 10 mm in diameter. Warming was underway in the 160-cm-thick sea ice beneath the melting snow. In the upper 50 cm of the underlying ice, temperatures were between −2°C and 0°C and salinities ranged from 1 to 4 ‰; giving brine volumes of 15–25%. The ice consisted primarily of columnar congelation ice, with the exception of the top 10 cm of the ice, which was granular. By a depth of 15 cm the c axes of the columnar ice crystals were oriented in the horizontal plane and by 70 cm the c axes became aligned in the horizontal plane parallel to the shore in the direction of the prevailing current [*Weeks and Gow*, 1978]. The melt pond case was measured at roughly the same location the day after the melting snow case. It consisted of 6 cm of water on top of 160 cm of melting ice and had a deep, bluish green color. The physical properties of the underlying ice were the same as in the melting snow example. Bare first-year ice was measured in early May of 1994, near the end of the growth season, in the Beaufort Sea at Barrow, Alaska. The ice was 172 cm thick, and though it was warming, it had not undergone any surface melting. Brine volumes were 6–7% in the interior of the ice, increasing to 13% near the bottom. Structurally, the ice cover consisted of columnar congelation ice, with a 10-cm-thick fine-grained surface layer. The c axes of the ice crystals were oriented in the horizontal plane and also aligned parallel to the direction of the ocean current.

3.3. Albedos and Reflectances

Total and spectral albedos were measured for each of the six cases. These results are comparable to those observed by previous researchers for similar ice types [*Grenfell and Maykut*, 1977; *Perovich and Grenfell*, 1981; *Grenfell and Perovich*, 1984; *Allison et al.*, 1993; *Perovich*, 1994, 1996]. Total albedos ranged from 0.16 for the ponded ice to 0.74 for the dry snow (Table 2). Spectral albedos are plotted in Figure 3, along with nadir reflectances. Albedos for cold snow are large (~0.9) and spectrally uniform. As the snow begins to melt, liquid water is present and the grain size and density increase. This results in a decrease in total albedo from 0.74 to 0.60 and a spectral decrease of 0.1 in the visible (500 nm) and 0.3 in the near-

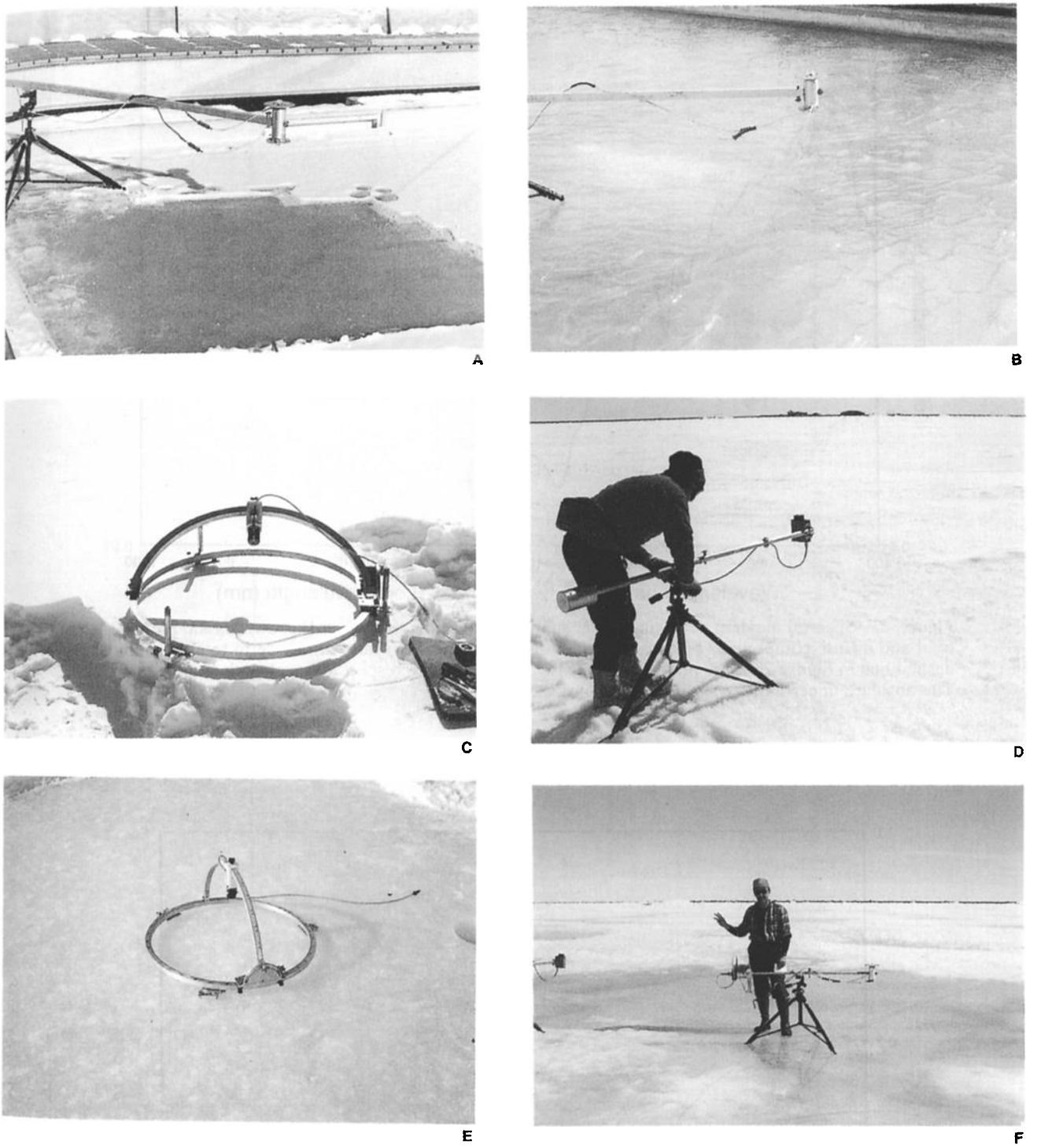

Plate 1. The six ice types studied: (a) young columnar ice, (b) pancake ice, (c) dry snow, (d) melting snow, (e) bare ice, and (f) melt pond.

infrared (1000 nm). Total and spectral albedos for pancake ice ($\alpha_T = 0.18$) were less than values for columnar ice ($\alpha_T = 0.32$) of the same thickness. There was less scattering in the upper few centimeters of the pancake ice owing to weathering and retexturing of the pancake ice, which resulted in a surface layer with relatively few air bubbles and brine pockets. Spectral albedos for the pancakes were fairly low, approximately 0.3, and constant at visible wavelengths, giving the pancakes a grayish appearance. The small albedo for ponded ice demonstrates the large impact of surface conditions on albedo. In this case a thin, 6-cm-thick layer of surface water reduced the albedo by more than 50% compared with bare ice. The nadir reflectance curves are similar in spectral shape to the albedo curves but are displaced in magnitude. Nadir reflectance is slightly larger than albedo for dry snow but is less for the other five cases.

Reflectances measured at 550 nm for five different azimuth angles and three different zenith angles are plotted in Figure 4a. Except for 0° azimuth, the observed angular variability in reflectance was less than 20% for all six snow and ice cases.

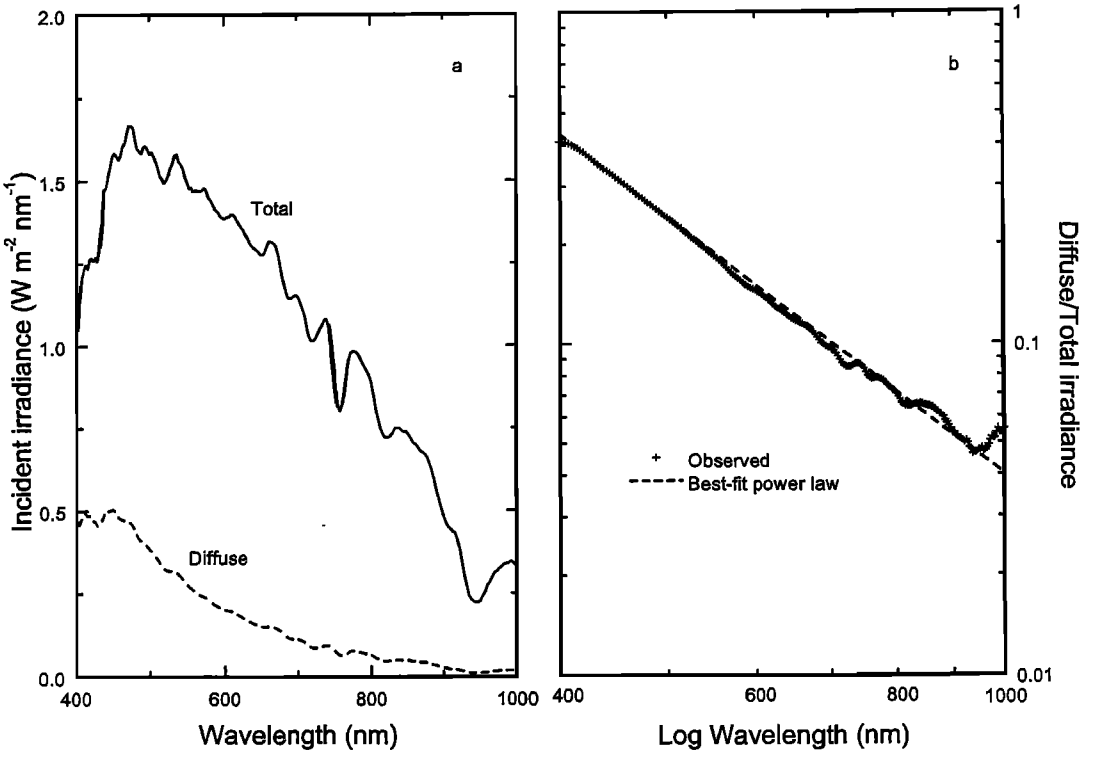

Figure 2. Spectral incident irradiance under sunny skies on June 8, 1995, at Barrow, Alaska. Plotted are (a) total and diffuse components of spectral incident irradiance, and (b) ratio of diffuse to total irradiance. The dashed line in Figure 2b is the power law decrease of the ratio with respect to wavelength (exponent = −2.8). The absolute uncertainty in incident irradiance was 15%.

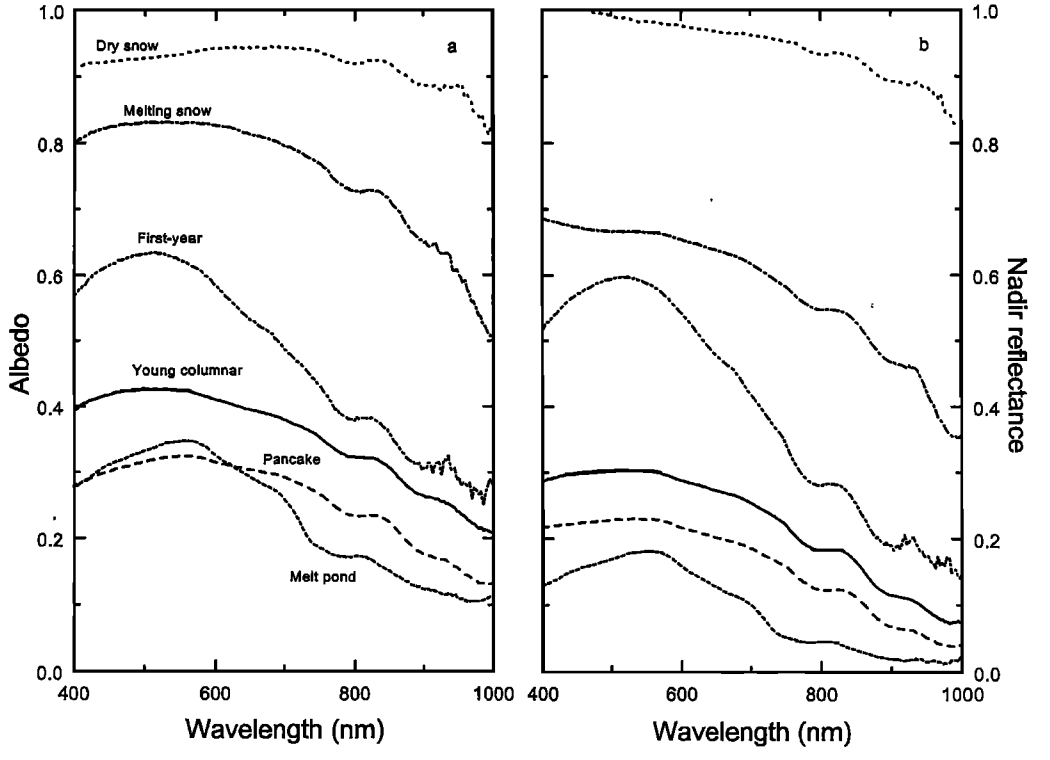

Figure 3. Spectral values of (a) albedo and (b) nadir reflectance for young columnar ice, pancake ice, cold snow, melting snow, cold bare ice, and ponded ice.

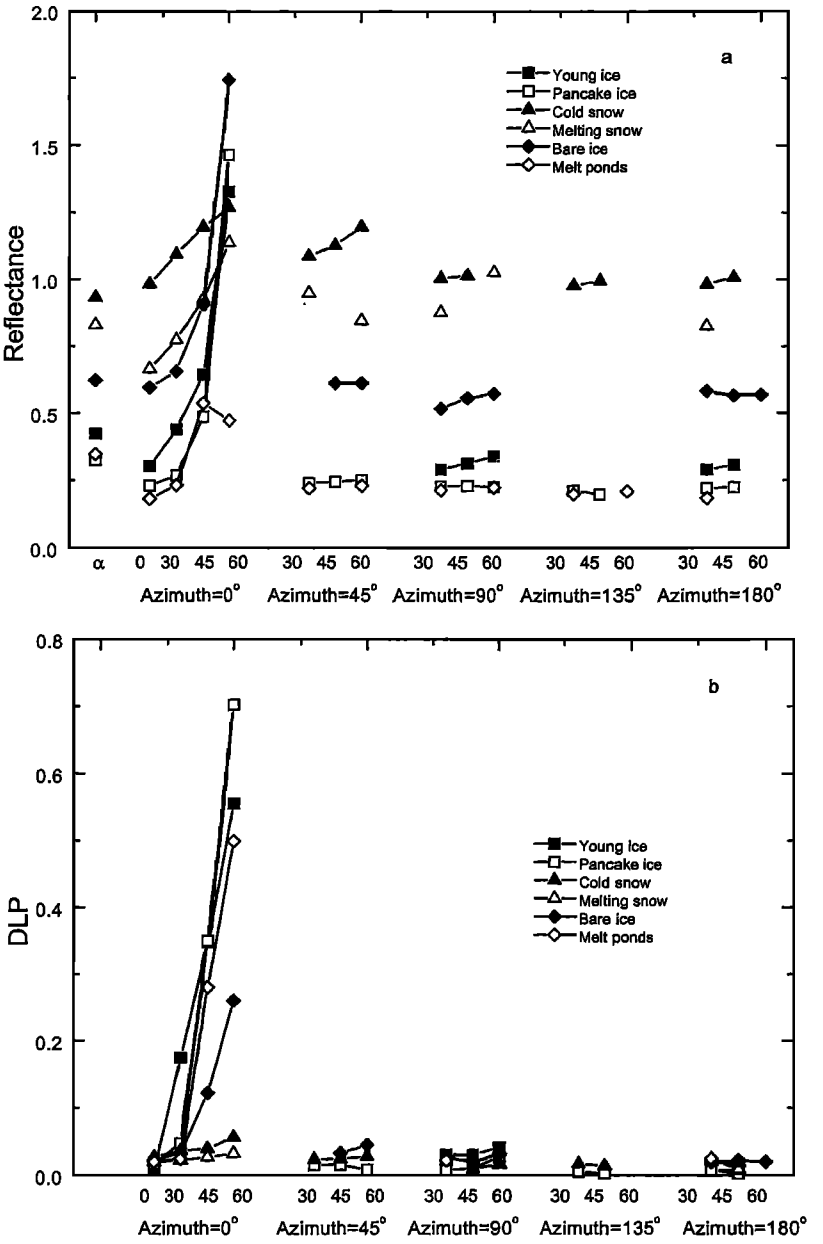

Figure 4. Angular distribution of (a) reflectance and (b) degree of linear polarization at 550 nm for young columnar ice, pancake ice, cold snow, melting snow, cold bare ice, and ponded ice.

The figure demonstrates that by far the greatest variability in the angular distribution of reflected radiance is at 0° azimuth, in the plane of incidence of the incident solar beam. Reflectances at 0° azimuth increased sharply with zenith angle, with smoother surfaces generally exhibiting a greater increase. For example, the observed increase from nadir to 60° zenith angle was 30% for dry snow, 50% for melting snow, 200% for bare ice, 450% for the columnar ice and the ponded ice and 600% for the pancake ice. Measurements at other wavelengths are consistent with this pattern; maximum variability of reflected radiance with zenith angle at 0° azimuth.

In Figure 4b the degree of linear polarization at 550 nm for the six cases is plotted for the same zenith and azimuth angles. As was the case for reflectance, the largest polarization occurs in the plane of incidence, with polarization increasing with zenith angle. Away from the plane of incidence ($\phi > 45°$), the reflected light is largely unpolarized, with the degree of linear polarization less than 0.04. These results indicate that the greatest changes in reflectance and polarization occur in the plane of reflection, with little variability at other azimuth angles. Because of this, we will concentrate on observations made in the plane of incidence.

3.4. Stokes Vector

The Stokes vector of the reflected light was measured at selected azimuth and zenith angles. Some background is needed before examining the Stokes vector results. In order to qualitatively interpret the results, we need to consider the polarization of the incident irradiance, as well as specularly reflected and volume-scattered light. The incident light field consists of a direct-beam solar component plus a diffuse component from the sky. The direct beam component is unpolar-

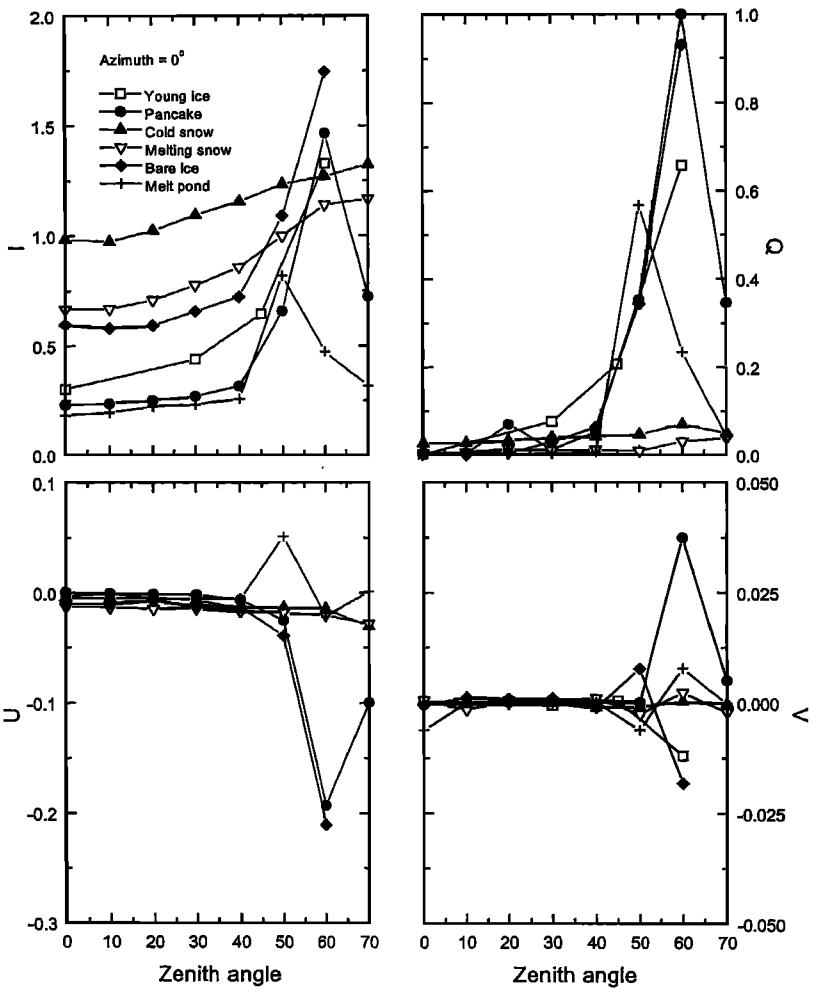

Figure 5. Four components of the Stokes vector at 550 nm at 0° azimuth for zenith angles from 0° to 70°. Data are reported for young columnar ice, pancake ice, cold snow, melting snow, cold bare ice, and a melt pond.

ized, as is the diffuse sky component except for a small portion perpendicular to the solar beam [*Minnaert*, 1954; *Bohren and Huffman*, 1983]. As Figure 2 indicates, the direct solar beam accounts for most of the incident solar radiation, ranging from 60% at 400 nm to 95% at 1000 nm. These factors imply that the incident solar radiation is largely unpolarized. However, Figure 4b shows that for several cases there is strong polarization of the light reflected in the plane of incidence. This can be explained by realizing that the reflected light consists of an unpolarized, volume-scattered component from the interior of the ice and a partially polarized, specularly reflected component of the direct beam. If the solar zenith angle is equal to Brewster's angle θ_B, then the specularly reflected light is completely polarized. Brewster's angle is defined as $\tan^{-1}(n_i/n_a)$, where n_i and n_a are the index of refraction of ice (1.31) and air (1.00) [*Jenkins and White*, 1976]. For an air-ice interface, θ_B is equal to 53°. All cases discussed in this paper have solar zenith angles close to θ_B (within 15°), and consequently, the specularly reflected light from the solar beam is highly polarized, with polarizations ranging from 66% to 98%. Since n_i is a weak function of wavelength in the visible and near-infrared, we can assume that the degree of polarization of the reflected direct beam is nearly constant with wavelength. This high degree of polarization provides a telltale signature of the contribution due to specular reflection of the solar beam.

The four components of the Stokes vector measured as a function of zenith angle at 0° azimuth are presented in Figure 5 for young ice, pancake ice, cold snow, melting snow, bare ice, and ponded ice. The plotted results are for a wavelength of 550 nm, which is the center wavelength for the circular polarization filter. Absorption coefficients for snow and ice are relatively small at 550 nm [*Grenfell and Maykut*, 1977; *Grenfell and Perovich*, 1981].

Examining the Stokes vector results, we can see that in general, the maximum observed reflectance and polarization was at θ = 50° or 60°, depending on the solar zenith angle (Table 2). The largest value of I was for the bare ice, and the largest percent increase was for the glazed pancake ice. The percent increase in I between the nadir value and the peak value ranged from 40% for cold snow to 540% for the glazed pancake ice. Note that in both the cold and melting snow cases, I continued increasing to θ = 70°, but the polarization (Q, U, and V) did not. This implies that the increase in I with zenith angle is due to multiple forward scattering, rather than specular reflection, of the solar beam. This result is consistent with

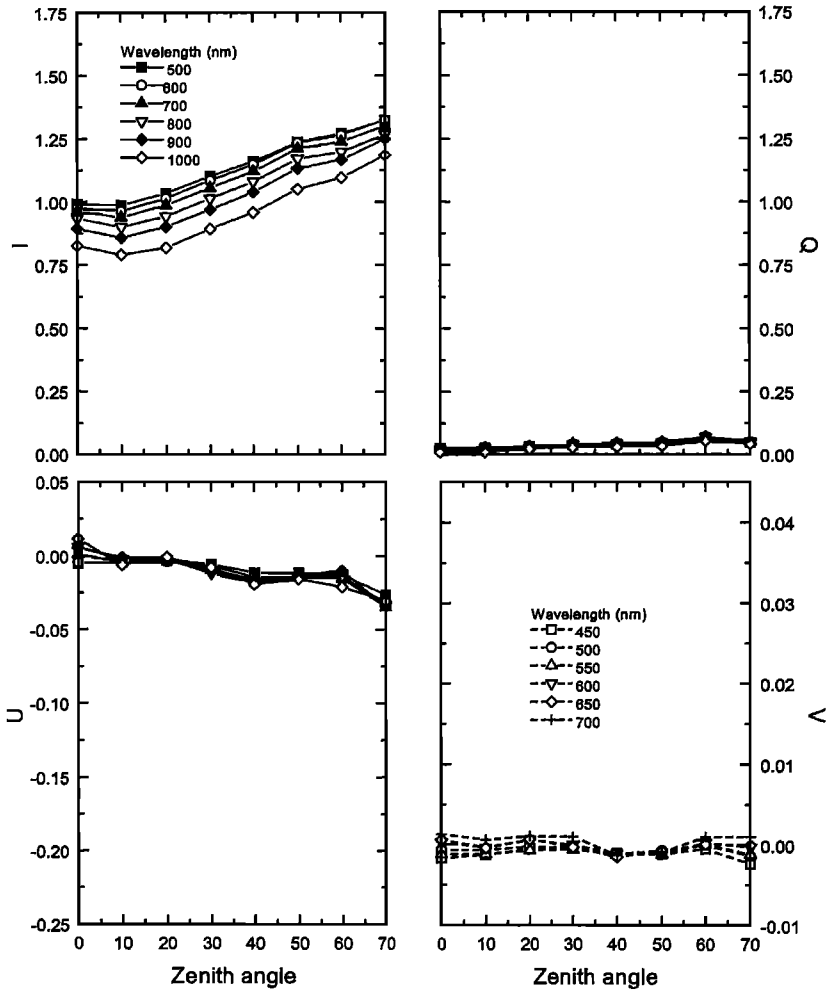

Figure 6. Spectral values of the Stokes vector for dry snow at 0° azimuth for zenith angles from 0° to 70°. Note that the vertical scales for I, Q, U, and V are different.

previous snow observations made at South Pole by *Grenfell et al.* [1994].

The dependence of Q on zenith angle was similar to that of I, with Q increasing in conjunction with I. The increase in Q with zenith angle was smallest for the snow cases and largest, with a peak value of 1, for the pancake case. There was little elliptical polarization (U), aside from a modest amount for the pancake and bare ice cases at $\theta = 60°$. Circular polarization (V) was near zero at all angles for all cases, except for pancake ice at $\phi = 0°$, $\theta = 60°$, where it was 0.04. The results in Figure 5 indicate that at 550 nm there is an increase in I and Q near the angle of reflection of the incident solar beam (θ_{rs}). The increase is greater for cases with a smooth surface, such as glazed pancakes, bare ice, and melt ponds, and much smaller for the cold and melting snow cases with their "rougher" surfaces.

We now examine the spectral dependence of the Stokes vector in the plane of incidence for two examples: cold snow (Figure 6) and pancake ice (Figure 7). These cases cover the full range of surface conditions from a rough surface with little specular reflection to a smooth surface with a sizeable specular component. For snow there are no major spectral changes evident in the Stokes vector as a function of wavelength. I increases with zenith angle roughly proportionally at all wavelengths. Polarization was small at all angles and all wavelengths, with values of Q, U, and V near zero from 500 to 1000 nm. Even near the angle of reflection, Q was less than 0.07 at all wavelengths, indicating that the specular component was a minor part of the reflected light.

The situation was quite different for the pancake ice. Not only is there a large increase in I with zenith angle, but the increase is greater at longer wavelengths. As Figure 7 shows, for zenith angles from 0° to 50°, peak values of I were at 500–600 nm, with I decreasing at longer wavelengths. However, for $\theta = 60°$ this behavior is reversed, with the largest values of I at longer wavelengths. The polarization components display a similar spectral behavior. Values of Q, U, and V at all wavelengths are near zero for zenith angles from 0° to 40°. Polarization then increases, reaching a maximum at $\theta = 60°$, with the increase being greatest at 1000 nm and smallest at 500 nm. This can be explained by considering the relative contributions of specular reflectance and volume scattering at different wavelengths. Extinction coefficients for sea ice are larger at 1000 nm than at 500 nm [*Grenfell and Maykut*, 1977; *Grenfell and Perovich*, 1981], and consequently, the contribution to reflection of light backscattered from within the ice is less. This is evident in the decrease in albedo with wavelength for the pancake ice. Since the magnitude of specular reflection

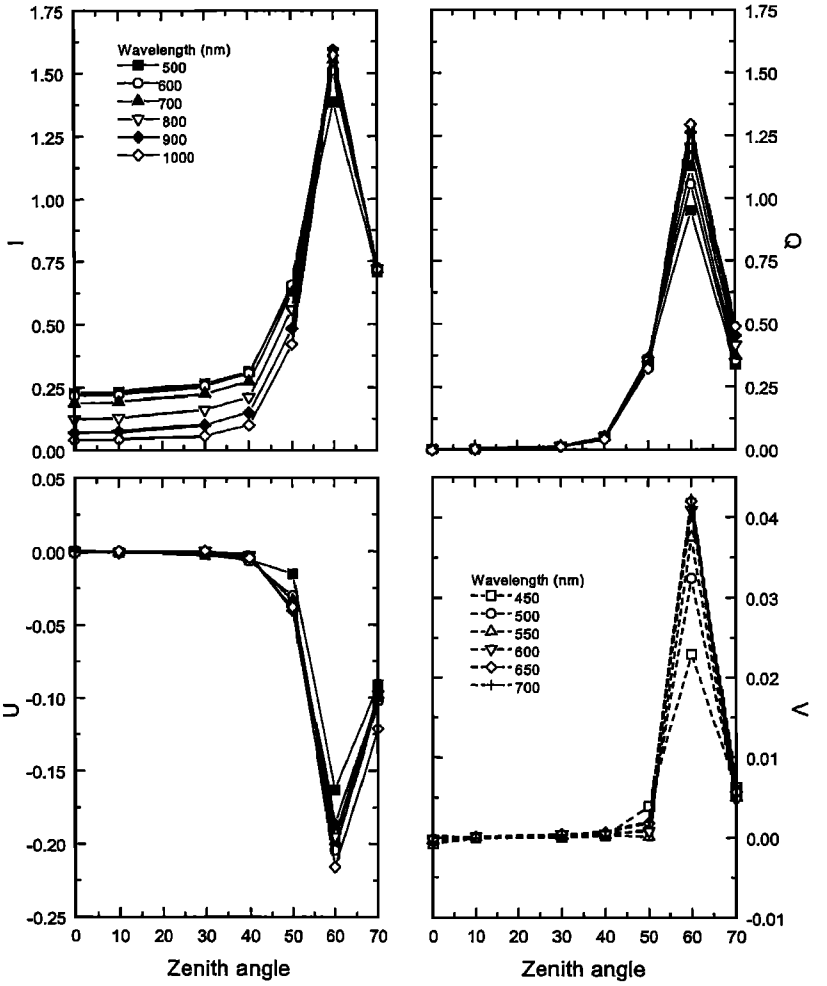

Figure 7. Spectral values of the Stokes vector for pancake ice at 0° azimuth for zenith angles from 0° to 70°. Note that the vertical scales for I, Q, U, and V are different.

is roughly independent of wavelength, it is a larger portion of the reflected light at longer wavelengths. As the specular component is polarized, the polarization of the reflected light is also greater at longer wavelengths. In general, for the cases with smooth surfaces there was a peak in the Stokes vector near the angle of reflection for the solar beam. This peak was associated with specular reflection and was more pronounced at longer wavelengths.

The results indicate that the greatest changes in the Stokes vector occur in the plane of incidence of the solar beam and that peak values were found in the observations made closest to the angle of reflection of the solar beam (θ_{rs}). Since θ_{rs} is close to Brewster's angle θ_B, any specularly reflected light is highly polarized, and the Stokes vector can give insight into the relative contributions of surface and volume scattering. Spectral values of reflectance I and the degree of linear polarization near θ_{rs} for the six cases are plotted in Figure 8. In all cases the reflectance at this angle is greater than the albedo, showing that there is some enhancement of the reflected radiance field in the forward direction. The fractional increase is smallest for the snow cases, and the degree of linear polarization is less than 0.1, implying that, as expected, there is little specular reflection from the snow and that the enhanced I results from multiple forward scattering of the solar beam. For the snow-free cases the forward enhancement of the reflected light is much greater, and there is significant polarization. Comparing the bare ice with the young ice and the pancake ice, there is a continual increase in I and in polarization at all wavelengths, indicating an increase in the contribution of specular reflection. This behavior is consistent with the physical properties of the ice for these three cases. We would expect the volume scattering to be greatest for the bare ice, since as a result of drainage, the upper 10 cm had a large number of air bubbles, and with a thickness of 170 cm it was optically thick at all wavelengths. The young ice and the pancake ice were much thinner than the bare ice and were not optically thick for wavelengths less than 700 nm. The ice was 15 cm thick in both cases, but the top few centimeters of young ice had a large number of brine pockets, while this portion of the pancakes had retextured into relatively clear ice with few inclusions. For these three cases there is a steady increase in the degree of linear polarization with wavelength. As before, since extinction coefficients for sea ice increase with wavelength [*Grenfell and Maykut*, 1977; *Grenfell and Perovich*, 1984], the amount of volume scattering would decrease. Thus there is a steady increase in the relative contribution of specular reflection and polarization with increasing wavelength.

The most extreme, and illustrative, results are for the melt

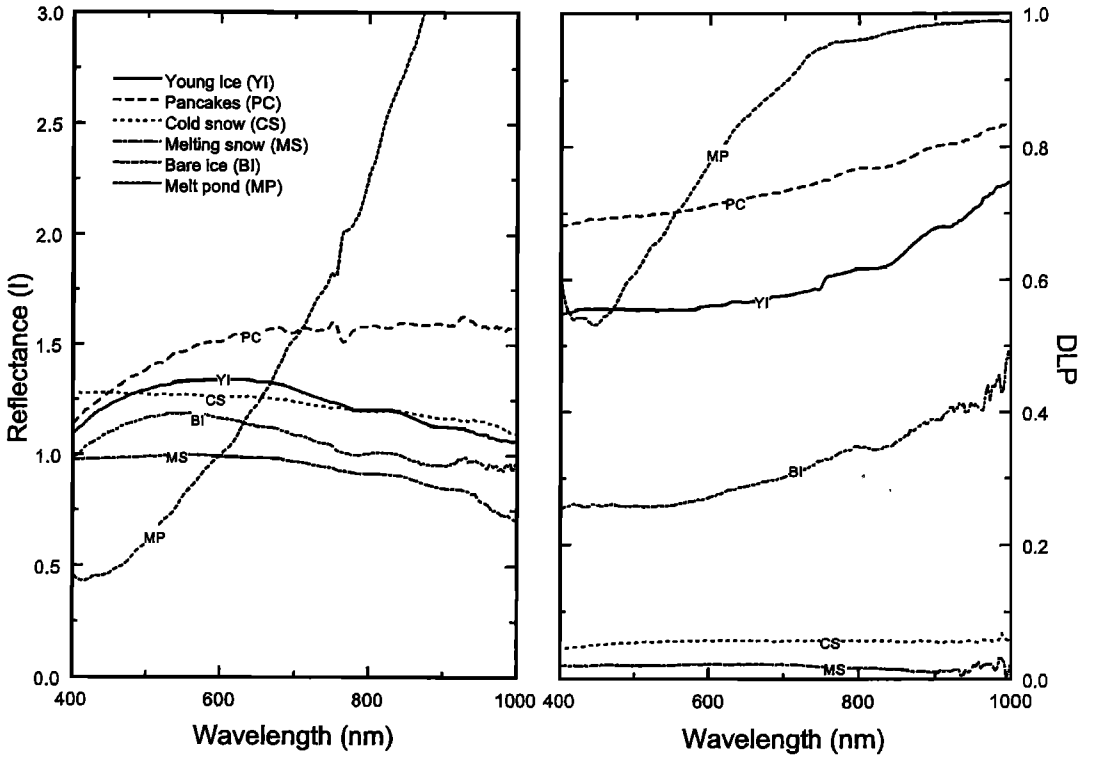

Figure 8. Spectral values of (a) reflectance and (b) degree of linear polarization for young columnar ice, pancake ice, cold snow, melting snow, cold bare ice, and ponded ice at the angle of observed maximum reflectance.

pond case, where the reflectance and polarization exhibit a very pronounced wavelength dependence. Reflectance increases sharply with wavelength from 0.5 at 500 nm to 5 at 1000 nm. There was a corresponding increase in polarization, and by 800 nm the reflected light was almost completely polarized. Again, this is consistent with the physical properties. The pond surface was flat and smooth, providing a good interface for specular reflection. Compared to the highly scattering ice, the pond water can be considered as a nonscattering, absorbing surface layer. Interpretation of melt pond albedos [*Grenfell and Maykut*, 1977; *Grenfell and Perovich*, 1984; *Perovich*, 1994] has suggested that at longer wavelengths, absorption in the water layer is great enough that the underlying ice does not contribute to the reflected irradiance and the reflected irradiance is due solely to specular reflection. The high reflectance and polarization at longer wavelengths of our pond results confirm this. The melt pond case provides a vivid demonstration of how Stokes vector measurements are influenced by the scattering and absorption in the medium. From 400 nm to 700 nm the melt pond polarization curve (Figure 8b) has the same spectral shape as the absorption curve for water. They both have a minimum near 450 nm and increase rapidly with wavelength. The increased absorption reduces the volume-scattering contribution, thereby enhancing the specular contribution and the polarization of the reflected light.

The spectral and angular Stokes vector observations can be explained qualitatively in terms of the physical and optical properties of the ice and snow. An intriguing possibility is whether the Stokes observations could be used to infer quantitative information on the physical and optical properties of the ice, in particular regarding scattering in the ice. An inadequate description of scattering is a major limitation in current sea ice radiative transfer models. Since sea ice is a highly scattering medium, direct measurement of scattering coefficients and phase functions is not possible. By linking spectral Stokes vector observations of the reflected radiance field with forward and inverse radiative transfer models, it may be possible to indirectly determine these quantities. Also, since absorption in the ice is wavelength dependent, results from different wavelengths could be combined to obtain information regarding scattering, and therefore ice conditions, at different depths in the upper portion of the ice.

3.5. Rough Versus Smooth Surface

Results from the young ice, pancake ice, snow-covered ice, bare ice, and ponded ice cases indicated that the light reflected from smooth surfaces had a larger specular contribution and greater polarization than that reflected from rough surfaces. However, the situation was complicated by the fact that the amount of volume scattering was also different for each of the cases. We were able to conduct an experiment where the effects of surface roughness were isolated. This was done by artificially roughening part of a 31-cm-thick, smooth, young ice sheet. The roughening was done by covering half of the ice surface with small pieces of ice that were a few millimeters in diameter. Spectral results are summarized in Figure 9 in plots of albedo, reflectance, and degree of linear polarization at an angle of 0° azimuth, 60° zenith. This particular angle was selected to illustrate the maximum differences between the two cases. A comparison of the results for the rough and smooth cases shows that the albedo was larger at all wavelengths for the rough case, while the reflectance and degree of linear

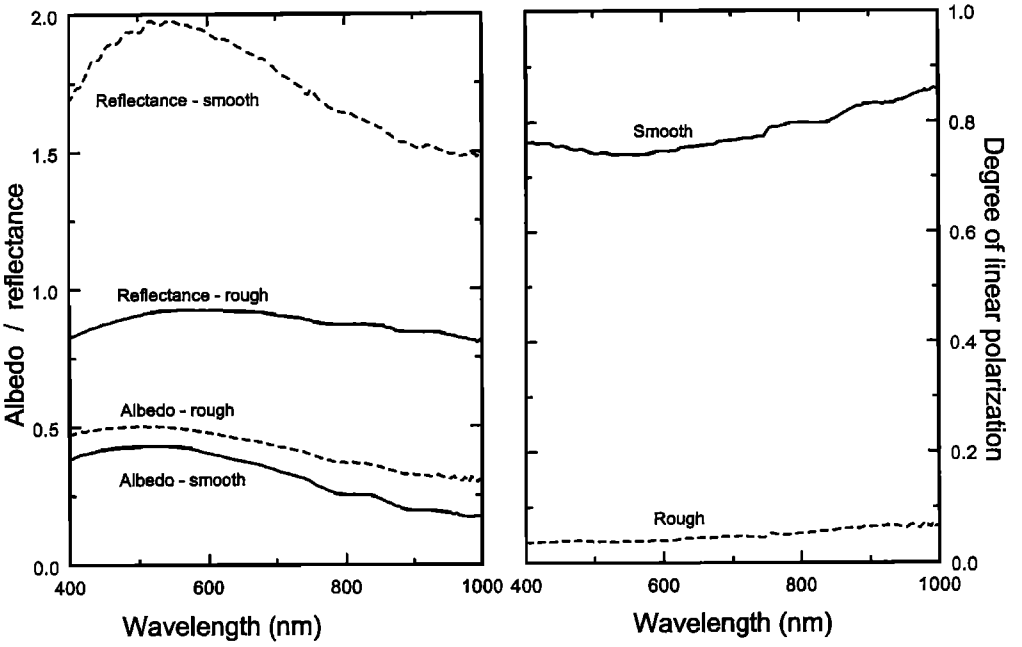

Figure 9. Spectral values of (a) albedo and reflectance and (b) degree of linear polarization for smooth, young ice and rough, young ice at $\theta = 60°$, $\phi = 0°$.

polarization at $\theta = 0°$, $\phi = 60°$ were much greater for the smooth surface. The process of adding roughness elements caused air to be entrained in the surface layer, resulting in increased scattering and albedo. At $\theta = 0°$, $\phi = 60°$, the reflected light from the smooth ice had a large specular component, as evidenced by the enhanced reflectance and the high degree of linear polarization. Reflectance at this angle was much lower for the rough ice, approximately half that of the smooth case. The small amount of polarization for the rough case implies that the specular component was small.

4. Conclusions

The spectral and total albedo observations reported in this paper show a strong sensitivity of albedo to surface conditions and are consistent with earlier studies. Stokes vector observations indicated that the greatest changes in reflectance and polarization occurred in the plane of incidence of the solar beam ($\phi = 0°$). Reflectances increased sharply with zenith angle, with smoother surfaces such as melt ponds, retextured pancakes, and bare ice generally exhibiting a larger increase than the snow cases with their "rougher" surfaces. For the smooth cases, peak values were found in the observations made closest to the angle of reflection of the solar beam (θ_{rs}). Since the solar zenith angle was close to Brewster's angle, any specularly reflected light was highly polarized. In the "smooth" ice cases there was significant polarization associated with the increase in reflectance, implying a substantial contribution from specular reflection. The increase in reflectance and degree of polarization near θ_{rs} was greater at longer wavelengths, where specular reflection was a larger component of the reflected radiance. For the snow cases, reflectance increased with zenith angle, but the polarization of the reflected light was less than 4%. This argues that the increase is due to multiple forward scattering, rather than specular reflection, of the solar beam. Away from the plane of incidence (>45°), the Stokes vector showed little angular dependence, and the reflected light at these angles was largely unpolarized, with the degree of linear polarization less than 0.04.

Angular and spectral variations in the Stokes vector for different ice types can be explained in terms of the physical and optical properties of the ice. The challenge for the future is to couple these observations with forward and inverse theoretical models to extract quantitative information regarding scattering in the ice and on the physical properties of the upper portion of the ice. The wavelength dependence of absorption in the ice may be exploited by combining results from different wavelengths to obtain information regarding scattering, and therefore ice conditions, at different depths in the upper portion of the ice.

Acknowledgments. I thank T. C. Grenfell for helpful discussions on light reflection and polarization. I appreciate the valuable contributions made by B. Elder and J. Govoni to the field measurement program. This work was funded by the Office of Naval Research, Ocean Optics Program, as part of an accelerated research initiative on the electromagnetic properties of sea ice under contract N00014-95MP-30002.

References

Allison, I., R. E. Brandt, and S. G. Warren, East Antarctic sea ice: Albedo, thickness distribution and snow cover, *J. Geophys. Res.*, *98*, 12,417–12,429, 1993.

Bohren, C. F., and D. R. Huffman, *Absorption and Scattering of Light by Small Particles*, John Wiley, New York, 1983.

Buckley, R. G., and H. J. Trodahl, Thermally driven changes in the optical properties of sea ice, *Cold Reg. Sci. Technol.*, *14*, 201–204, 1987.

Dirmhirn, I., and F. D. Eaton, Some characteristics of the albedo of snow, *J. Appl. Meteorol.*, *14*, 375–379, 1975.

Dozier, J., R. E. Davis, A. T. C. Chang, and K. Brown, The spectral bidirectional reflectance of snow, in *Proceedings of the 4th International Colloquium on Spectral Signatures of Objects in Remote Sensing, Eur. Space Agency Spec. Publ., ESA SP-287*, 87–92, 1988.

Ebert, E. E., and J. A. Curry, An intermediate one-dimensional thermodynamic sea ice model for investigating ice-atmosphere interactions, *J. Geophys. Res.*, *98*, 10,085–10,109, 1993.

Ebert, E. E., J. L. Schramm, and J. A. Curry, Disposition of solar radiation in sea ice and the upper ocean, *J. Geophys. Res.*, *100*, 15,965–15,975, 1995.

Grenfell, T. C., A theoretical model of the optical properties of sea ice in the visible and near infrared, *J. Geophys. Res.*, *88*, 9723–9735, 1983.

Grenfell, T. C., Radiative transfer model for sea ice with vertical structure variations, *J. Geophys. Res.*, *96*, 16,991–17,001, 1991.

Grenfell, T. C., Analysis of surface-based passive microwave observations during LEADEX 1992, *Digest, International Geoscience and Remote Sensing Symposium (IGARRS '94), IEEE Publ. 94CH3378-7*, 1005–1007, Inst. of Elec. and Electron. Eng., New York, 1994.

Grenfell, T. C., and G. A. Maykut, The optical properties of ice and snow in the Arctic Basin, *J. Glaciol.*, *18*, 445–463, 1977.

Grenfell, T. C., and D. K. Perovich, Radiation absorption coefficients of polycrystalline ice from 400–1400 nm, *J. Geophys. Res.*, *86*, 7447–7450, 1981.

Grenfell, T. C., and D. K. Perovich, Spectral albedos of sea ice and incident solar irradiance in the southern Beaufort Sea, *J. Geophys. Res.*, *89*, 3573–3580, 1984.

Grenfell, T. C., S. G. Warren, and P. C. Mullen, Reflection of solar radiation by the Antarctic snow surface at ultraviolet, visible and near-infrared wavelengths, *J. Geophys. Res.*, *99*, 18,669–18,684, 1994.

Hunt, A. J., D. Miller, and M. S. Quinby-Hunt, Polarization-dependent measurements of sea ice, in *Ocean Optics 12*, edited by J. S. Jaffe, *Proc. SPIE Int. Soc. Opt. Eng.*, *2258*, 613–622, 1994.

Jenkins, F. A., and H. E. White, *Fundamentals of Optics*, McGraw-Hill, New York, 1976.

Jin, Z., K. Stamnes, and W. F. Weeks, The effect of sea ice on the solar energy budget in the atmosphere–sea ice–ocean system: A model study, *J. Geophys. Res.*, *99*, 25,281–25,294, 1994.

Kuhn, M., Bidirectional reflectance of polar and alpine snow surfaces, *Ann. Glaciol.*, *6*, 164–167, 1985.

Langleben, M. P., Albedo and degree of puddling of a melting cover of sea ice, *J. Glaciol.*, *8*, 407–412, 1969.

Langleben, M. P., Albedo of melting sea ice in the southern Beaufort Sea, *J. Glaciol.*, *10*, 101–104, 1971.

Maykut, G. A., and N. Untersteiner, Some results from a time dependent, thermodynamic model of sea ice, *J. Geophys. Res.*, *76*, 1550–1575, 1971.

Miller, D., M. S. Quinby-Hunt, and A. J. Hunt, A novel bistatic polarization nephelometer for probing scattering through a planar interface, *Rev. Sci. Instrum.*, *67*, 2089–2095, 1996.

Miller, D., M. S. Quinby-Hunt, and A. J. Hunt, Laboratory studies of the angle and polarization dependent light scattering in sea ice, *Appl. Opt.*, *36*, 1278–1288, 1997.

Minnaert, M., *The Nature of Light and Color in the Open Air*, 362 pp., Dover, Mineola, N. Y., 1954.

Perovich, D. K., Theoretical estimates of light reflection and transmission by spatially complex and temporally varying sea ice covers, *J. Geophys. Res.*, *95*, 9557–9567, 1990.

Perovich, D. K., Seasonal changes in sea ice optical properties during fall freeze-up, *Cold Reg. Sci. Technol.*, *19*, 261–273, 1991.

Perovich, D. K., Light reflection from sea ice during the onset of melt, *J. Geophys. Res.*, *99*, 3351–3359, 1994.

Perovich, D. K., *The Optical Properties of Sea Ice*, *CRREL Monogr. 96-1*, 25 pp., U.S. Army Cold Reg. Res. and Eng. Lab., Hanover, N. H., 1996.

Perovich, D. K., and T. C. Grenfell, Laboratory studies of the optical properties of young sea ice, *J. Glaciol.*, *27*, 331–346, 1981.

Schlosser, E., Optical studies of Antarctic sea ice, *Cold Reg. Sci. Technol.*, *15*, 289–293, 1988.

Steffen, K., Bidirectional reflectance of snow at 500–600 nm, in *Large Scale Effects of Seasonal Snowcover*, *IAHS Publ.*, *166*, 415–425, 1987.

Tucker, W. B., III, A. J. Gow, and W. F. Weeks, Physical properties of summer sea ice in the Fram Strait, *J. Geophys. Res.*, *92*, 6787–6803, 1987.

Warren, S. G., Optical properties of snow, *Rev. Geophys.*, *20*, 67–89, 1982.

Weeks, W. F., and S. F. Ackley, The growth, structure, and properties of sea ice, *CRREL Monogr. 82-1*, 130 pp., U.S. Army Cold Reg. Res. and Eng. Lab., Hanover, N. H., 1982.

Weeks, W. F., and A. J. Gow, Preferred crystal orientations in the fast ice along the margins of the Arctic Ocean, *J. Geophys. Res.*, *83*, 5105–5121, 1978.

D. K. Perovich, U.S. Army Cold Regions Research and Engineering Laboratory, 72 Lyme Road, Hanover, NH 03755. (e-mail: perovich@hanover-crrel.army.mil)

(Received November 1, 1996; revised May 14, 1997; accepted May 30, 1997.)